A Comparative Study on the Performance of CFD/LBM-DEM Coupling in Predicting Soil Fluidization

Thanh T. Nguyen, Ph.D., M. ASCE[1], Buddhima Indraratna, Ph.D., F. ASCE[2], Cholachat Rujikiatkamjorn[3], Ph.D., M. ASCE, Shay Haq[4]

[1] Research Fellow, Transport Research Centre, University of Technology Sydney, NSW 2007, Australia; Email: thanh.nguyen-4@uts.edu.au
[2] Distinguished Professor, Director of Transport Research Centre, University of Technology Sydney, NSW 2007, Australia; Email: buddhima.indraratna@uts.edu.au
[3] Professor, Transport Research Centre, University of Technology Sydney, NSW 2007, Australia; Email: cholachat.rujikiatkamjorn@uts.edu.au
[4] PhD candidate, Transport Research Centre, University of Technology Sydney, NSW 2007, Australia; Email: shay.haq@student.uts.edu.au

ABSTRACT

Coupling Discrete Element Method (DEM) with Computational Fluid Dynamics including Navier-Stokes theories (CFD-DEM) and Lattice Botlzemann Method (LBM-DEM) has been used widely to model the response of soil foundation under increasing seepage flows, however, a comparison of these methods in predicting soil and fluid behaviours during fluidization has not been carried out in a rigorous way. The current paper will hence provide an evaluation on their performance by applying them to model a laboratory test where a sandy soil is subjected to fluidization process under increasing hydraulic gradient. A brief discussion about the differences in their theories and numerical algorithm is made before the DEM is used to simulate a representative soil element while NS-based CFD and LBM are used separately to model upward fluid flows. The mutual interactions between fluid and solid phases are carried out and update to each other through third-party platforms. The results show relatively similar hydraulic conductivity predicted by the two methods, which agrees well with the experimental data, however, the critical hydraulic gradient estimated by LBM-DEM coupling is found closer to the experimental value. The CFD-DEM coupling provides more stable computation through its averaged fluid variables, whereas LBM-DEM coupling can provide more detailed interactions between fluid and soil particles at micro-scale due to its high resolution. The study then suggests several conditions which can optimize the efficiency of using these methods in practical applications.

INTRODUCTION

Rising seepage flow can occur under soil foundations due to the build-up of excess pore water pressure subjected to external loads such as transport, earthquake and preloading embankments, causing internal erosion, heave and fluidization failures (Hayashi and Shahu 2000; Duong et al. 2014; Kuo et al. 2017; Nguyen et al. 2019). Conventional studies (Duong et al. 2014; Fleshman and Rice 2014) normally use laboratory and analytical methods to assess soil behaviour under increasing upward flow, while recent attention has gone to capturing micro-scale responses based on advanced computational methods that facilitates our insightful understanding of the failures. Discrete Element Method (DEM) has been

coupled with Computational Fluid Dynamics (CFD) to investigate soil and fluid behaviours at micro-scale in recent years, among which two approaches, i.e., DEM coupled with Navier-Stokes (NS)-based CFD (normally referred to as CFD-DEM coupling) and Lattice Boltzmann Method (i.e., LBM-DEM coupling) are usually preferred. These approaches have shown considerable success in modelling the migration of particles under hydraulic flows, however, there is a lack of comparative study which elaborates their capabilities as well as limitations.

In this paper, the two fluid-particle coupling methods, i.e., CFD-DEM and LBM-DEM are adopted to simulate soil fluidization under increasing hydraulic gradient. The model results are validated with experimental data, while their performances are evaluated in detail. This analysis will advance our understanding of these two computational methods, facilitating our choice of model in practice.

OVERVIEW OF THEORETICAL BACKGROUND

For the sake of brevity, only the major theoretical concepts and key differences between CFD-DEM and LBM-DEM couplings are presented in this section. Other details can be found in past studies (Kloss et al. 2012; Seil et al. 2018; Nguyen and Indraratna 2020a; Indraratna et al. 2021).

Discrete element method (DEM)

The governing equations of DEM can be given by

$$m_i \frac{d\boldsymbol{U}_{pi}}{dt} = \sum_{j=1}^{n_i^c} \boldsymbol{F}_{cij} + \boldsymbol{F}_{gi} + \boldsymbol{F}_{fi} \quad \textbf{(1)}$$

$$I_i \frac{\omega_{pi}}{dt} = \sum_{j=1}^{n_i^c} (M_{c,ij} + M_{r,ij}) \quad \textbf{(2)}$$

where $\boldsymbol{U}_{pi}$ and ω_{pi} are the translational and angular velocities of particle i, respectively while m_i is the solid particle mass; $\boldsymbol{F}_{c,ij}$ and $M_{c,ij}$ are the contact force and torque acting on particle i by particle j (or walls) with n_i^c denoting the number of total contacts of particle i; t is the time, while $\boldsymbol{F}_{g,i}$ is the gravitational force and I_i is the inertia moment of particle i. $M_{r,ij}$ is the rolling friction torque. The total hydraulic force $\boldsymbol{F}_{f,i}$ includes different components such as the drag, the pressure gradient and viscous forces induced by fluid on particle i. The subscripts p and f denote particle and fluid, respectively.

In the above, the influence of fluid on solid particle behaviour is represented through the fluid-particle interaction force $\boldsymbol{F}_{f,i}$ which can be computed from fluid computation side (i.e., CFD and the third party) and incorporated into DEM over time (Figure 1). Other details of particles contacts and rolling friction, especially in modelling granular soils can be found in previous studies (Nguyen and Indraratna 2020b).

Coupling DEM with CFD based on Navier-Stokes (NS) theories

In order to consider the effect of solid particles, the governing NS equations are modified as follows:

$$\frac{\partial n_f}{\partial t} + \nabla.\left(n_f \boldsymbol{U}_f\right) = 0 \tag{3}$$

$$\frac{\partial(\rho_f n_f \boldsymbol{U}_f)}{\partial t} + \nabla.\left(\rho_f n_f \boldsymbol{U}_f \boldsymbol{U}_f\right) = -n_f \nabla p\mathbf{I} + \nabla.\left(n_f \boldsymbol{\tau}_f\right) + \rho_f n_f \boldsymbol{g} - \boldsymbol{f}_p \tag{4}$$

where n_f is the porosity of a fluid cell with n denoting the overall porosity in the computed domain while $\rho_f, \boldsymbol{\tau}_f, \boldsymbol{U}_f$ and p are the density, viscous stress, velocity and pressure of fluid, respectively; $\mathbf{I}$ is the identity tensor; $\boldsymbol{g}$ is the gravitational acceleration vector; $\boldsymbol{f_p}$ is the mean volumetric particle-fluid interaction force which represents the effect of solid particles on the fluid phase.

The most common method that facilitates coupling fluid with solid phases, while solving the fluid equations, is the Finite Volume Method, FVM (OpenFOAM). In this solution, the fluid domain is discretised into a finite number of cells where the governing equations are solved locally using the averaged fluid velocity and pressure. Each fluid cell can contain a number of soil particles that requires the fluid cell to be bigger than the largest soil particles, thus the term coarse grid or unresolved techniques. The averaged fluid variables are used to estimate fluid forces acting on particles, it hence reduces computational cost. The mean volumetric particle-fluid interaction force $\boldsymbol{f_p}$ in a fluid cell is calculated by:

$$\boldsymbol{f}_p = \sum_{i=1}^{n_p} \varpi_i \left(\frac{\boldsymbol{F}_{fi}}{V_c}\right) \tag{5}$$

where n_p is the number of particles in the cell with a volume V_c; $\boldsymbol{F}_{fi}$ is the total hydraulic force induced by fluid acting on particle i.

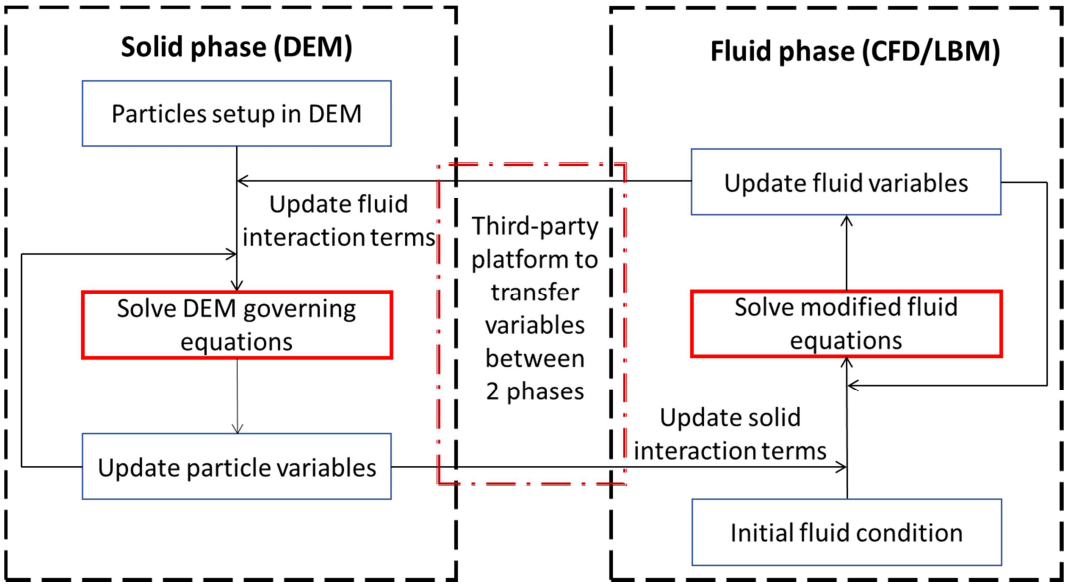

Figure 1. General algorithm of CFD-DEM and LBM-DEM coupling

Coupling DEM with LBM

In the Lattice Boltzmann Method (LBM), a fluid is assumed as a composite of particles in which their conservation in momentum and mass is governed through the density distribution function (i.e., $f_i(x,t)$) of particle streaming and collisions, which is

$$\underbrace{f_i(x+e_i\Delta_t, t+\Delta t)}_{streaming} = \underbrace{f_i(x,t) - \frac{1}{\tau}\left(f_i(x,t) - f_i^{eq}(x,t)\right)}_{collision} \quad \textbf{(6)}$$

Details of the above equation can be found in past studies (Seil et al. 2018). The influence of solid phase on this process of a fluid-solid system can be described by modifying Eq. (6) as follows:

$$f_i(x+e_i\Delta_t, t, +\Delta t) - f_i(x,t) = -\frac{1}{\tau_t}(1-B)\left(f_i(x,t) - f_i^{eq}(x,t)\right) + B\Omega_i^s \quad \textbf{(7)}$$

where *B* is the weighing function given by:

$$B\left(n_f, \tau_t\right) = \frac{\left(n_f - \frac{1}{2}\right)}{\left(1-n_f\right) + \left(\tau_t - \frac{1}{2}\right)} \quad \textbf{(8)}$$

where the porosity n_f can also be referred to as volumetric fraction and denoted as ε in some other studies (references). When n_f equals 0, the cell is completely filled with fluid, and Eq. (7) becomes the original equation which only considers fluid to fluid interaction (Eq. 6). The term τ_t is the dimensionless relaxation time. The newly introduced term Ω_i^s in Eq. (7) is the collision operator for fluid nodes that overlap with solids, which can be treated based on the bounce-back technique of non-equilibrium density distribution functions. Specific procedure to solve Eq. (6) and (7) can be found in past studies (Seil et al. 2018; Indraratna et al. 2021).

On the other hand, the influence of fluid on solid particles in DEM can be captured through the hydrodynamic force which can be computed as follows:

$$F_f = \sum_{n_s} B_{n_s} \sum_i \Omega_i^s \, c_i \quad \textbf{(9)}$$

Meanwhile, the hydrodynamic torque T_f can be given by:

$$T_f = \sum_{n_s} \left(x_{n_s} - x_c\right) \times \left(B_{n_s} \sum_i \Omega_i^s c_i\right) \quad \textbf{(10)}$$

where n_s is the number of lattice cells covered by the solid particle, x_n are the coordinates of the lattice node n^{th} and x_c is the centre of mass of the solid particle.

Boundary treatment of fluid-solid phases

In the unresolved CFD-DEM coupling, particles can be divided into different small parts and their contributions to the solid fraction of fluid cells are evaluated depending on the location of divided portions (i.e., divided void fraction technique). It is noteworthy that there are also other boundary techniques such as the centre void fraction and immerse boundary techniques which can also be applied for CFD-DEM coupling. The current study used the divided void fraction technique as this is one of the most preferable approaches in current practice. For LBM-DEM coupling, because the fluid cells are much finer than the particle size, immersed moving boundary (IMB), which can capture more accurately the solid/fluid fraction at

boundaries, was used in the present investigation. Further details of these techniques can be found in past studies (Seil et al. 2018; Nguyen and Indraratna 2020a; Indraratna et al. 2021).

The current study used DEM based on LIGGGHTS, while NS-based CFD and LBM were implemented on OpenFOAM and Palabos. Their coupling was made through open-source platforms CFDEM and LBDEM (Kloss et al. 2012; Seil et al. 2018).

COMPARISON OF CFD-DEM vs. LBM-DEM COUPLING MODELS

This section aims to examine the performance of CFD-DEM (unresolved) and LBM-DEM coupling in simulating soil fluidization under increasing seepage flow. Two benchmark cases of soil fluidization with (*i*) gas and (*ii*) water flows, which are commonly used in previous numerical studies, are adopted to examine the two numerical approaches.

Experimental investigation on soil fluidization

An experiment was carried out to observe how soil would respond to increasing seepage flow and the results were then used to validate numerical simulations. A coarse sand which is commonly used as filter layer (e.g., sand blanket) across different foundations was adopted for this experiment (Figure 2). The sand was filled into a transparent cell without compaction (i.e., loose state) and then subjected to an upward flow. The initial porosity of soil was estimated based on the dry mass and the height of soil specimen. The input hydraulic gradient (*i*) was controlled via a water tank with adjustable height, while a porous plate was placed at the bottom to ensure the uniform distribution of fluid at the inlet. Manometers were used to measure the water heads along the soil specimen that enabled the hydraulic gradient to be computed. A stationary high-resolution camera was used to record the soil response through the transparent cell. Soil deformation (e.g., heave at the surface) can then be estimated using the recorded video based on image processing. The input *i* was increased gradually while the outlet velocity was recorded over time until the soil could not resist the flow (i.e., the outlet flow velocity swiftly increased).

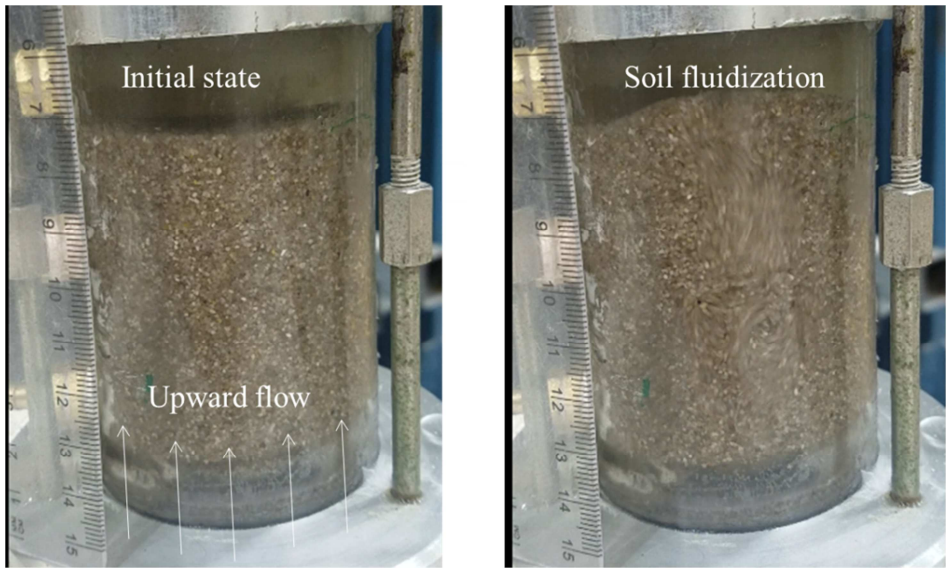

Figure 2. Experiment to examine soil fluidization under upward seepage flow

It is noteworthy that the same concept has also been used in past studies to investigate soil fluidization under rising seepage flows. Soil properties such as porosity and particles size can be different across various studies, while the fluid can vary from water to gas to examine different contexts of soil fluidization such as under transport, dam and mining activities.

Numerical model setup

Table 1 Numerical parameters for modelling

Input parameters	Gas-induced fluidization (Case *i*)- validated with past studies	Fluid-induced fluidization (Case *ii*)- current study
Size of particle domain (mm)	W100 x H221 x T24	W16 x HT23.9 x T16
Young's modulus (Pa)	$8x10^6$	$8x10^6$
Friction coefficient (sliding)	0.5	0.5
Rolling friction coefficient	0.1	0.1
Viscosity of gas/fluid (Pa.s)	1.8	10.04×10^{-4}
Density of solid particles (kg/m^3)	2500	2650
Density of gas/fluid (kg/m^3)	1.2	1000
Particle diameter (mm)	4	0.6 to 1.8
Porosity	0.43	0.38-0.39
Boundary type	Rigid walls	Periodic boundary

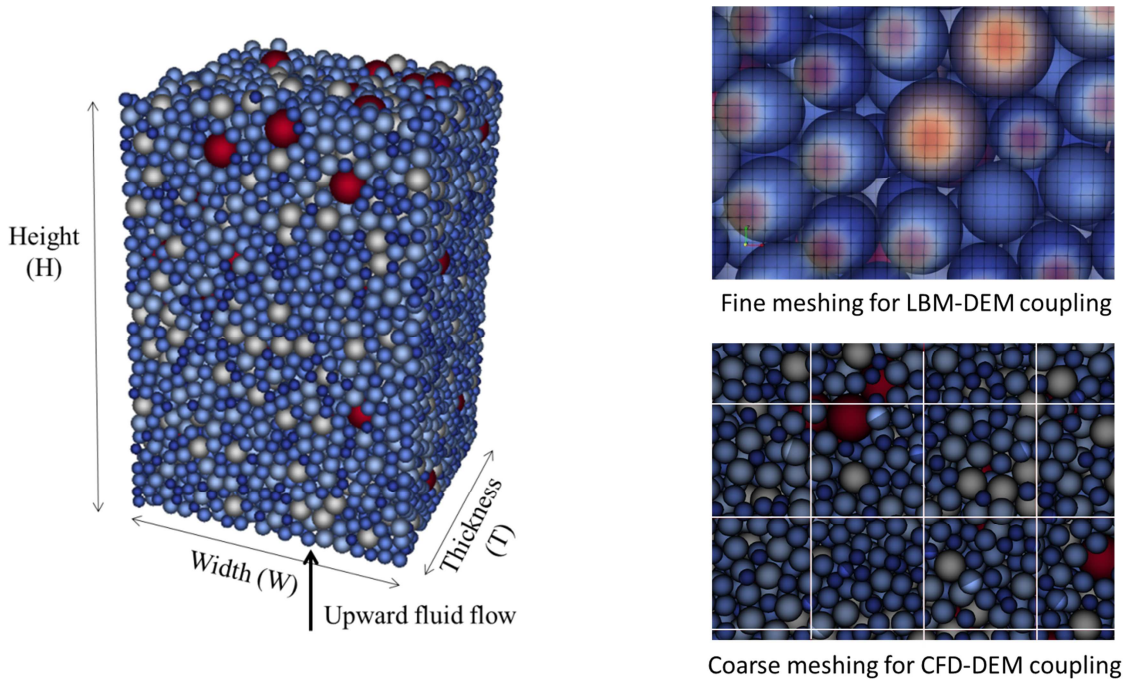

Figure 3. a) A typical soil specimen subjected to upward gas/fluid flow; b) meshing of fluid domain in comparison to particle size

Particles were generated in DEM and stabilized under gravity. The particle size was selected with respect to the particle size distribution (PSD). Periodic boundary was used to simulate a soil element located at the middle of the experimental soil specimen (i.e., soil-to-soil interaction). Rolling and sliding friction coefficients were adopted with respect to past DEM models of sandy soils. The porosity of specimen was controlled by manipulating the friction coefficients while particles settling. It is noteworthy that Young's modulus was scaled down to enhance the computational efficiency, which has been proved to not affect significantly the model outcomes as the soil was not compressed (i.e., unloading) in the present study.

The fluid flow was applied under a different pressure between the bottom and surface of the soil specimen. This pressure was increased gradually, thus increasing hydraulic gradient (i.e., the ratio between the pressure difference and the height). The surface (superficial) flow velocity was computed by CFD/LBM, while soil behaviour (e.g., particle migration and porosity) and interstitial flow characteristics were also captured. For CFD-DEM coupling, the fluid cells was at least twice the largest soil particles, while for LBM-DEM coupling, the smallest soil particles were at least 5 times larger than the fluid cells. Figure 3 represents a typical soil element generated in DEM and the meshing ratios of fluid domain in comparison to the solid particles.

RESULTS AND DISCUSSION

Case *i*: Fluidization induced by gas flow- validation with past studies

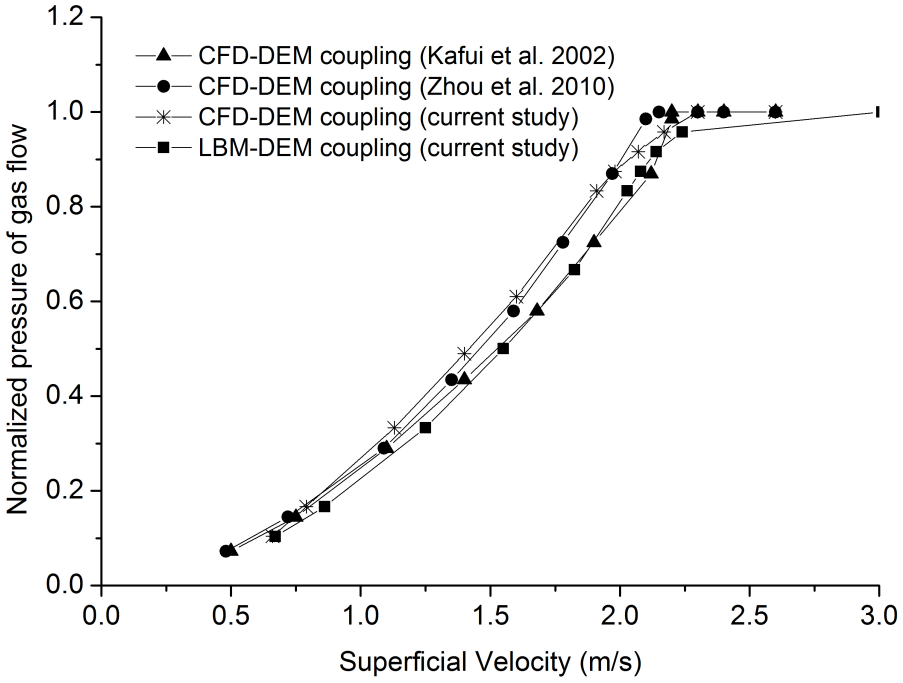

Figure 4. Flow velocity with increasing pressure-validation with previous models

In this investigation, soil fluidization occurs under a gas flow, which has been used widely to validate multiphase computations in various past studies (Kafui et al. 2002; Zhou et al. 2010). Computational parameters for the model are shown in Table 1. Rigid walls were used in this case to be consistent with past numerical simulations. Figure 4 shows the results computed by the current numerical methods compared to past CFD-DEM coupling studies. The current

CFD-DEM model agrees very well with Zhou et al. (2010), whereas there is a certain deviation between these curves with those predicted by Kafui et al. (2002) and LBM-DEM coupling technique. For example, at a superficial velocity of 1.75 m/s, the predicted pressures by the current CFD-DEM coupling and Zhou et al. (2010) are larger, resulting in later fluidization (i.e., where the velocity increases rapidly without change in flow pressure). This is understandable because Zhou et al. (2010) has significantly modified fluid-particle interaction forces from Kafui et al. (2002), while the theoretical framework of the current CFD-DEM coupling, i.e., the original CFDEM codes developed by Kloss et al. (2012) is mainly adopted from Zhou et al. (2010).

Case *ii*: Fluidization induced by water flow-comparison with current experimental data

Figure 5 represents the predicted hydraulic curves (discharge velocity over i) compared to experimental data obtained from the current and past investigations (Fleshman and Rice 2014). In these simulations, periodic boundary was employed, and the numerical parameters are shown in Table 1. Generally, the predicted results agree relatively well with the experimental data, given the wide range that the hydraulic conductivity of geomaterials usually varies in (e.g., in the order of 10^{-2} to 10^{-5} for sandy soils). At the onset of fluidization, the discharge velocity increases swiftly, which represents the critical level of hydraulic gradient i_c. Interestingly, CFD-DEM coupling results in a larger value of i_c (i.e., 1.47) compared to LBM-DEM coupling (i_c = 1.2), which means a more accurate outcome given by the combined LBM-DEM technique. Indeed, the larger magnitude of i_c predicted by the unresolved CFD-DEM coupling in comparison with conventional experimental data has been reported in several past studies. The reason might come from the average fluid variables used in the coarse meshing technique of this approach, whereas LBM-DEM coupling uses significantly finer mesh associated with higher computational cost.

Figure 6 shows how the coupled CFD-DEM and LBM-DEM techniques can capture the interstitial fluid flow at different degrees of hydraulic gradient. Obviously with much finer resolution, LBM-DEM coupling can present in detail the difference in fluid velocity between voids which are smaller than soil particles. For example, the fluid flowing around particles and the centroid of pore throats can be estimated, thus better representing how fluid becomes turbulent at the onset of fluidization where porous system begins to break severely. As CFD-DEM coupling used large fluid cells with averaged variables, it cannot show in detail how the seepage develops during soil fluidization. In fact, the localized and micro-scale behaviour of fluid and particles cannot be predicted well due to the average fluid-particle interaction terms being used in this approach.

The computed heave formation (i.e., particles rising under seepage flow) by both solutions agreed relatively well with experimental observation. The predicted results showed that the soil surface can rise about 5 to 6% compared to its original level, which was slightly larger than the measured value (i.e., 4.5%) right before the inception of fluidization. For brevity, these data are not included in this paper, further details can be found in an independent study by the Authors (Nguyen and Indraratna 2022).

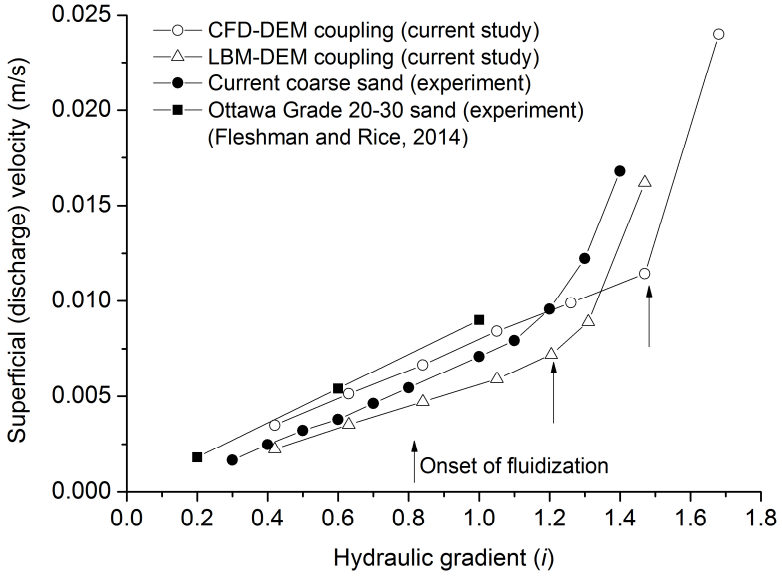

Figure 5. Predicted hydraulic curves in comparison to experimental data

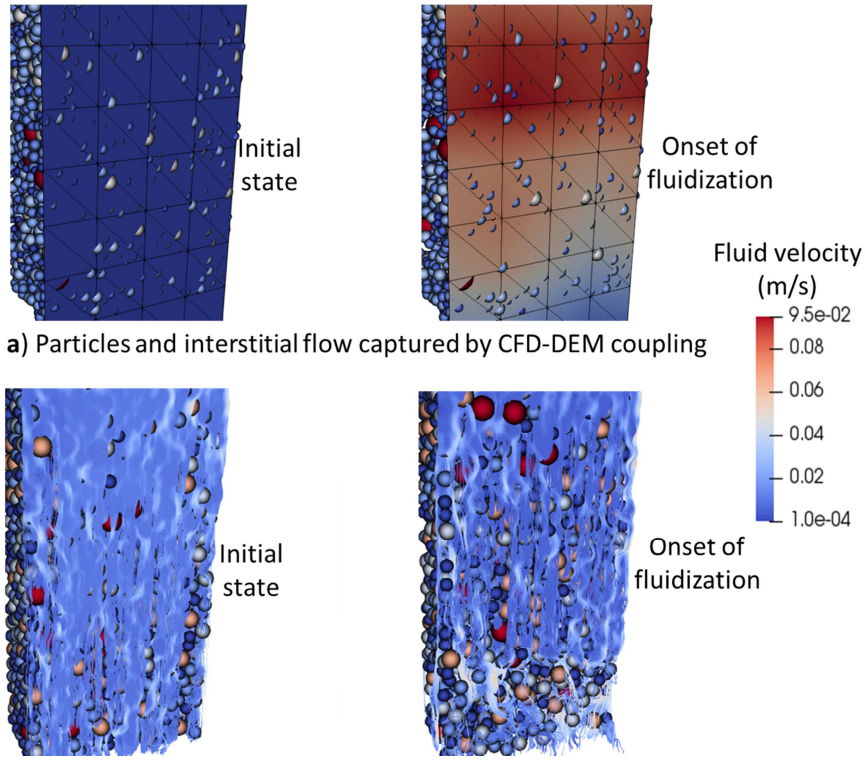

Figure 6. Computed interstitial fluid flow at the middle slice of soil specimen

CONCLUSIONS

The current paper compares two different fluid-particle coupling techniques, i.e., CFD-DEM based on Navier-Stokes theories and LBM-DEM based on Lattice Boltzmann method in modelling soil fluidization. The results showed that the two examined coupling techniques can predict relatively well soil fluidization under upward flows of water and gas. The critical hydraulic gradient i_c predicted by LBM-DEM coupling was closer to the experimental data, and this method can capture in detail the micro-scale evolution of interstitial fluid. However,

as using a high number of fluid cells, LBM-DEM coupling was relatively expensive in computation, thus it is relevant to investigate small size specimens with major focus on micro-scale (i.e., less than 5-10 times the average particle size) behaviour. On the other hand, the unresolved CFD-DEM coupling is more time-effective and reasonable to simulate meso- to macro-scale specimens/issues.

ACKNOWLEDGEMENT

This research was supported by the Australian Government (ARC-**LP160101254**), Transport Research Centre (TRC-UTS), SMEC, Coffey, ACRI and Sydney Trains is much appreciated.

REFERENCES

Duong, T.V., Cui, Y.-J., Tang, A.M., Dupla, J.-C., Canou, J., Calon, N. and Robinet, A. 2014. Investigating the mud pumping and interlayer creation phenomena in railway sub-structure. Engineering Geology, **171**: 45-58. doi: https://doi.org/10.1016/j.enggeo.2013.12.016.

Fleshman, M.S. and Rice, J.D. 2014. Laboratory modeling of the mechanisms of piping erosion initiation. Journal of Geotechnical & Geoenvironmental Engineering, **140**(6): 04014017:1-12.

Hayashi, S. and Shahu, J.T. 2000. Mud pumping problem in tunnels on erosive soil deposits. Géotechnique, **50**(4): 393-408. doi: 10.1680/geot.2000.50.4.393.

Indraratna, B., Phan, N.M., Nguyen, T.T. and Huang, J. 2021. Simulating Subgrade Soil Fluidization Using LBM-DEM Coupling. International Journal of Geomechanics, **21**(5): 04021039. doi: doi:10.1061/(ASCE)GM.1943-5622.0001997.

Kafui, K.D., Thornton, C. and Adams, M.J. 2002. Discrete particle-continuum fluid modelling of gas–solid fluidised beds. Chemical Engineering Science, **57**(13): 2395-2410.

Kloss, C., Goniva, C., Hager, A., Amberger, S. and Pirker, S. 2012. Models, algorithms and validation for opensource dem and cfdem. Progress in Computational Fluid Dynamics, an International Journal, **12**(2): 140-152.

Kuo, C., Hsu, C., Wu, C., Liu, P. and Chen, D. 2017. Study on the piping path and mechanism of mud pumping in railway subgrade. *In Proceedings of the* 19th International Conference on Soil Mechanics and Geotechnical Engineering (ISSMGE), Seoul. pp. 1051-1054.

Nguyen, T.T. and Indraratna, B. 2020a. A coupled CFD-DEM approach to examine the hydraulic critical state of soil under increasing hydraulic gradient. ASCE International Journal of Geomechanics, **20**(9): 04020138-1:15. doi: https://doi.org/10.1061/(ASCE)GM.1943-5622.0001782.

Nguyen, T.T. and Indraratna, B. 2020b. The energy transformation of internal erosion based on fluid-particle coupling. Computers and Geotechnics, **121**: 103475. doi: https://doi.org/10.1016/j.compgeo.2020.103475.

Nguyen, T.T. and Indraratna, B. 2022. Fluidization of soil under increasing seepage flow: an energy perspective through CFD-DEM coupling. Granular Matter, **(In Press)**. doi: 10.1007/s10035-022-01242-6.

Nguyen, T.T., Indraratna, B., Kelly, R., Phan, N.M. and Haryono, F. 2019. Mud pumping under railtracks: Mechanisms, Assessments and Solutions. Australian Geomechanics Journal, **54**(4): 59-80.

Seil, P., Pirker, S. and Lichtenegger, T. 2018. Onset of sediment transport in mono- and bidisperse beds under turbulent shear flow. Computational Particle Mechanics, **5**(2): 203-212. doi: 10.1007/s40571-017-0163-6.

Zhou, Z.Y., Kuang, S.B., Chu, K.W. and Yu, A.B. 2010. Discrete particle simulation of particle–fluid flow: model formulations and their applicability. Journal of Fluid Mechanics, **661**: 482-510. doi: doi:10.1017/S002211201000306X.